

Use of Finite Element Model and Temperature Measurements for Real Time Control of Active Surface and Pointing of a 50 m Radio Telescope


Frank W. Kan and Rajesh S. Rao

Simpson Gumpertz & Heger Inc.
297 Broadway, Arlington MA 02474

ABSTRACT

The Large Millimeter Telescope (LMT) is a 50 m diameter radio telescope with an actively controlled segmented surface to be used for astronomy at millimeter wave lengths. The specifications call for a surface accuracy of 70 micrometers RMS and a pointing accuracy of 0.7 arcseconds RMS. This paper evaluates a proposed approach for computing and correcting in real time the surface deformations of the primary reflector and the pointing errors of the telescope due to thermal deformations using a finite element model and temperature measurements throughout the telescope structure.

Key Words: LMT, finite element model, thermal deformations, surface accuracy, pointing accuracy

Further author information  www.sgh.com; Email: fwkan@sgh.com; Telephone: 781-643-2000; Fax: 781-643-2009

INTRODUCTION

The LMT/GTM (Large Millimeter Telescope / Gran Telescopio Milimetrico), a joint project of the University of Massachusetts and the Instituto Nacional de Astrofisica Optica y Electronica of Mexico, will be built at 4,600 m on a mountain in central Mexico. The LMT is a 50 m diameter radio telescope with an actively controlled segmented surface to be used for astronomy at millimeter wave lengths.

TELESCOPE STRUCTURE

The LMT telescope structure consists of two main parts: the elevation structure and the alidade structure. The function of the elevation structure is to support the primary reflector and the subreflector. The elevation structure itself is supported on the alidade structure. The elevation structure can be divided into three components: the backstructure which supports the primary reflector, the subreflector support structure, and the transition structure which provides the transition from the backstructure to the alidade structure. Figure 1 shows a schematic view of the elevation structure for the LMT preliminary design.

The primary reflector is a 50 m diameter paraboloid with f/D of 0.35. In the preliminary design, the primary reflector is an actively controlled surface made up of 126 hexagonal segments supported on actuators. Each segment is approximately 5 m across and is supported at three of the six vertices on actuators that are mounted on the front face of the backstructure. The backstructure is a space truss in which each joint on its front face supports an actuator. The truss configuration consists of a triangular grillage of trusses, with approximately half as many nodes on the back face as on the front face. The truss members are made up of circular and rectangular tube steel sections.

The subreflector support structure supports the subreflector, the subreflector positioner and the subreflector wobbler. It consists of a quadrupod with each of its four legs being a truss assembly built from wide flange steel sections. Each of the quadrupod legs is braced out of plane at two locations along its length by prestressed cables. The legs and bracing cables extend to outriggers outside the primary reflector surface.

The transition structure connects the backstructure to its support points on the alidade structure. It consists of the hexagonal ring beam and the elevation wheel structure. The hexagonal ring beam supports the backstructure at six locations. The perimeter and transverse members of the hexagonal ring beam are built-up box sections. Elevation stub shafts extend from the side members of the hexagonal ring beam, and support the entire elevation structure through the elevation bearings mounted on the alidade. The elevation wheel structure consists of the cone structure, the drive arc, the counterweight structure, and bracing members. The cone structure provides out of plane stiffness to the hexagonal ring beam and also serves to transfer the counterweight load to the hexagonal ring beam. Braces are used to restrain the counterweight mass and the drive arc. The counterweight structure consists of a steel box filled with concrete and is used to balance the telescope about its elevation axis. The elevation structure is driven at the drive arc by the elevation drives and pinions, which in turn are supported on the alidade.

The alidade structure supports the elevation structure through the elevation bearings, and houses both the elevation and azimuth drive systems. The alidade structure consists of rectangular tube steel sections that form a square base and two A-frames on the sides. The alidade structure is

supported vertically at the four corners by hydrostatic bearings. A pintle bearing provides lateral supports to the alidade and allows it to rotate about the vertical axis.

SURFACE ACCURACY

The LMT is to be operational at frequencies of up to 345 GHz ($\lambda = 0.87$ mm). This imposes a limitation on surface RMS error σ_s (deviation from the best-fit-paraboloid) of $\sigma_s/4 = 70$ μm . In addition to initial fabrication and alignment errors, the primary reflector surfaces distort due to gravity loads as the antenna rotates in elevation, due to changes in temperature distribution and due to wind loads if the antenna is exposed.

To achieve the required accuracy, the preliminary design of the primary reflector of the LMT (Figure 1) utilizes a novel approach with an actively controlled segmented surface with a real time closed loop control system. The 50 m diameter reflector consists of 126 hexagonal segments, each about 5 m across, supported on actuators (Figure 2). The Active Control System (ACS) utilizes edge sensors to measure the relative positions of adjacent segments and actuators to compensate for the deflections of the supporting structure, and thus maintains the reflector surface to the required accuracy. The active surface approach is derived from that first developed for use in the 10 m Keck optical telescope (Ref. 1). For the LMT, Simpson Gumpertz & Heger Inc. (SGH) proposed a modified concept, as shown in Figure 3, in which adjacent segments share actuators (Refs. 2 and 3). It has been shown that most of the errors that affect the performance of the active control system can be made acceptably small except for the effects of systematic deformations of the segments (Refs. 3 and 4). System deformations of the segments affect the displacements at the sensor mounting points so that the sensor readings do not represent the relative displacement of the surfaces of the segments. In particular, these systematic deformations of the segments will cause the control system to impose actuator motions that introduce errors in the surface which propagate and grow across the aperture.

To resolve the error propagation problem, a different approach was proposed in which the edge sensors would be eliminated and the actuators would be used in an open loop mode. The actuator motions required to compensate for gravity deformations would be based on results of finite element analyses adjusted by calibration using holography at two or more elevations. To correct for thermal effects, a thermal correction model would be used in which the temperatures of the members throughout the elevation structure would be measured and used with the finite element model to calculate the required actuator motions. In this paper, the thermal design which minimizes the temperature variations in the telescope structure is described and the feasibility of such a thermal correction model is evaluated.

POINTING

The nominal orientation of the antenna is measured by encoders. The actual pointing direction of the antenna is the direction of maximum gain, which depends on the direction of the axis of the best-fit paraboloid, and on the relative positions of the primary reflector, subreflector, and feed. Typically, by calibration and other means, a pointing bias model is developed to evaluate the repeatable differences between the direction given by the encoders and the direction of peak gain. The residual difference is the pointing error. Pointing errors are caused by the deformations of the backstructure, the subreflector support, and of the azimuth structure due to gravity loads as the antenna rotates in elevation, due to changes in temperature distribution and due to wind loads if the

antenna is exposed. Other sources of pointing error include tilt of the elevation encoder support, non-orthogonality of the azimuth and elevation axes, bearing run-out, and encoder errors. The pointing control system considered during the conceptual development of the LMT involved measuring the relative positions of the primary reflector, subreflector, and feed with respect to a reference platform near the intersection of the elevation and azimuth axes, and measuring the position of that platform with respect to ground. Because of the difficulty and cost of making these measurements with the required accuracy and speed, other approaches are being considered. One such approach uses a bias model to compensate for repeatable effects, a temperature measurement and correction model to account for thermal deformations, and recalibration by pointing to a known source every two hours. In this paper the feasibility of such a thermal correction model for pointing is evaluated.

THERMAL CORRECTION MODEL

In order to reduce the magnitude of the surface RMS errors and the pointing errors, a thermal correction model for the telescope structure will be used to account for, in real time, the temperature changes occurring in each of the members of the telescope.

In this approach, temperature sensors will be used to measure the temperatures in selected members of the telescope structure. The average temperature of all the members and the temperature gradient across the depth of beam members will be calculated (interpolated or extrapolated) based on the above temperature measurements. Using the changes in these temperatures, the thermal correction model will compute the thermal deformations of the elevation structure, and will compute the residual deformations of the primary reflector with respect to the best-fit surface at the actuator support points. The Active Control System (ACS) of the primary reflector will then use these residual displacements as input for an open-loop system and minimize the surface deviations. The thermal correction model will also calculate the change in direction of peak gain resulting from the rigid body rotation of the primary reflector with respect to the encoder, and the displacements and rotations of the subreflector with respect to the primary reflector.





For surface accuracy, the thermal correction model will be used to account for the temperature changes in the telescope between re-alignments of the segments using holography. For pointing, the thermal correction model will be used to account for temperature changes occurring in the two-hour period since the pointing system will be recalibrated every two hours by pointing the telescope to a known source.

The use of the thermal correction model will not completely eliminate the errors resulting from the thermal effect. The residual surface RMS error is the RMS of the difference between the actual surface deviation and the predicted (and correctable) surface deviation. The residual beam pointing error is the difference between the actual direction of peak gain and the predicted direction of peak gain. The residual surface RMS error or residual beam pointing error due to thermal effects of the telescope structure after application of the thermal correction model will be due to (a) the error in the temperature measurements, (b) the error in the member temperature predictions, and (c) the error in the temperature effect predictions. The first two errors can be combined to a single equivalent RMS temperature error on each individual member and the residual surface RMS error or residual beam pointing error is the sum of the contributions of all the individual members. The third error can be estimated as a percentage of the expected surface deviation or pointing correction predicted by the thermal correction model.

In this study, the effects of the thermal deformations of the subreflector support structure are compensated by a thermal correction model of its own. For brevity, the thermal correction model for the subreflector support structure is not discussed in details here. However, the general discussions regarding the thermal correction model for the elevation structure and the alidade also apply to that for the subreflector support structure.

ASSUMPTIONS

In calculating the surface accuracy, the direction of peak gain and their residual errors, the following assumptions were made:

-  Displacements of the primary reflector surface are taken as the displacements of the actuator support points.
-  Displacements of the actuator support points that are tangent to the surface will not affect the surface RMS error and the beam pointing error.
-  The actuators and the actuator motions are always normal to the surface.
-  When the active control system is in the closed loop mode, i.e., when it is using the edge sensors, it will not correct for rigid body motions of the primary reflector. In other words, the actuators will not be moved in any combination that results in rigid body motions of the primary: translation along z-axis, rotation about x-axis and rotation about y-axis (Figure 4).

FINITE ELEMENT MODEL OF TELESCOPE STRUCTURE

The thermal correction model described above involves performing structural analyses to calculate the deformation of the structure resulting from the measured temperature changes. The combined finite element model of telescope structure shown in Figure 4 was used to predict the effect of temperature change in each member. This model was also used for gravity and modal analyses (not discussed in this paper) to evaluate other aspects of the telescope performance.

The model consists of 664 nodes and 1678 elements. All members in the space truss that form the backstructure are modeled as rod elements (CROD). Each of the 126 hexagonal segments is represented by a single node at its center and is connected to the backstructure using a RBE3 element. Each hexagonal segment is supported in a statically determinate manner and does not affect the deformation of the backstructure resulting from thermal loading. The truss assemblies of the subreflector support structure are modeled using beam elements (CBAR). The prestressed cables that brace the truss assemblies are modeled as rod elements. In the transition structure, the hexagonal ring beam, the drive arc beam, and the counterweight structure are modeled by beam elements since they are designed to resist flexural loads. The cone structure and other braces are modeled by rod elements. The counterweight structure is connected to the drive arc beam using rigid elements (RBE2). All the members in the alidade structure are modeled by beam elements.

For each member in the elevation structure and the alidade structure, one or two unit temperature changes are applied as individual load cases. Uniform temperature changes are applied to all members, and for beam elements, changes in linear temperature gradient across the depth of the member are also applied.

A total of 1047 load cases in 25 runs were performed using MSC/NASTRAN. The process was automated by generating the input for the unit temperature changes through a BASIC program and by submitting MSC/NASTRAN through a BATCH command. A post-processing program was also developed to process the results of 1047 load cases.

EFFECTIVE SURFACE DEVIATION PREDICTED BY THERMAL CORRECTION MODEL

This section describes the procedure used to compute the required normal deformations at actuator support points to minimize surface deviations, and the procedure used to evaluate the residual surface RMS error after application of the thermal correction model.

The thermal correction model uses the temperature measurements in the elevation structure and computes the required normal deformations at the actuator support points to minimize surface deviations. For a given set of temperature measurements, the thermal correction model first extrapolates the temperature for all the members in the elevation structure, and then uses the results of the unit temperature load cases to compute the displacement normal to the surface at each actuator support point. The effective surface deviation (half RF pathlength error), e^0_j , at each corresponding surface node with respect to the best-fit paraboloid is calculated from the normal displacements. The best fit paraboloid is obtained by removing the rigid body components from the raw displacements and assuming that the subreflector can be displaced and rotated to an optimal position thereby minimizing the RMS of surface deviations. The procedure used to compute the best fit paraboloid and the optimal position of the subreflector is described in details in Ref. 5 and is not repeated here for brevity. The thermal correction model commands the actuators to correct for the residual effective surface deviation at each surface node, and this minimizes the surface RMS error.

The procedure to evaluate the residual surface RMS error after application of the thermal correction model involves computing the rate of change of surface RMS error for unit temperature in each of the members in the elevation structure. Consider a thermal loading state of the telescope at which the thermal deformations would result in effective surface deviation, $\mathbf{e}^0(\mathbf{r})$, on the primary reflector surface. The rate of change of the surface RMS error for a unit temperature change in a given member j is given by the following equation (Ref. 6):

$$\gamma_j = \frac{\mathbf{e}^0(\mathbf{r}) \mathbf{e}_j(\mathbf{r}) f(\mathbf{r}) dS}{\int_0 f(\mathbf{r}) dS}$$

where γ_j = rate of change of surface RMS error due to unit temperature change in member j
 γ^0 = surface RMS error due to the thermal loading state
 $\mathbf{e}_j(\mathbf{r})$ = vector of effective surface deviation due to unit temperature change in member j
 $\mathbf{e}^0(\mathbf{r})$ = vector of effective surface deviation due to the thermal loading state
 $f(\mathbf{r})$ = illumination function
 \mathbf{r} = position vector for a given point on the primary reflector surface

Discretizing the above equation in terms of effective surface deviations at each of the 147 surface nodes or actuator locations, the rate of change of surface RMS is given as:

$$j = \frac{\sum_{i=1}^{147} e_i^0 e_{ij} A_i}{\sum_{i=1}^{147} A_i}$$

- where γ_{oj} = rate of change of surface RMS error due to unit temperature change in member j
 γ_o^0 = surface RMS error due to the thermal loading state
 e_{ij} = effective surface deviation at surface node i due to unit temperature change in member j
 e_i^0 = effective surface deviation at surface node i due to the thermal loading state
 A_i = area/illumination function weighting factor for surface node i (an illumination function with a 12 dB taper was used in this study)

The rate of change of surface RMS error is a function of the existing thermal loading state of the telescope. It must be noted that the rate of change of surface RMS error does not depend on the actual magnitude of the temperatures but only on the shape of temperature distribution.

In this study, the following four thermal loading states were considered:

1. Thermal gradient of 0.05 °F/ft along x axis (elevation axis)
2. Thermal gradient of 0.05 °F/ft along y axis
3. Thermal gradient of 0.05 °F/ft along z axis (vertical)
4. Bilinear thermal gradient along z axis: 0.05 °F/ft below elevation axis and 0.1 °F/ft above elevation axis.

Figure 4 shows the orientation of the x, y and z axes along which thermal gradients are imposed on the structure.

The finite element model of the telescope structure described in the previous section was used to predict the effect of each of the four thermal loading states. A MSC/NASTRAN analysis was performed for each thermal loading state to calculate the normal displacement at each surface node. The effective surface deviation, e_i^0 , at each surface node with respect to the best-fit paraboloid was calculated from the normal displacements as discussed in the first part of this section.

The effect of temperature change in each member was also analyzed using the finite element model of telescope structure. For each member in the elevation structure, one or two unit temperature changes were applied as individual load cases. Uniform temperature changes were applied to all members, and for beam elements, changes in linear temperature gradient across the depth of the member were also applied. A total of 823 load cases in 20 runs were performed using MSC/NASTRAN. For each unit temperature load, the effective surface deviation e_{ij} at each surface node was calculated from the normal displacement.

The rate of change of the surface RMS error for a unit temperature change in member j was computed for each of the four thermal loading states. Combining the rate of change of surface RMS error with the errors in temperature measurement and prediction, the residual surface error due to thermal effects of the elevation structure after application of the thermal correction model can be evaluated.

DIRECTION OF PEAK GAIN PREDICTED BY THERMAL CORRECTION MODEL

This section describes the procedure used to compute the direction of peak gain predicted by the thermal correction model and the corresponding residual pointing error.

For a unit temperature change in member j within the elevation structure and the alidade, the direction of peak gain can be computed using a procedure similar to that described in Ref. 5. The rigid body rotations of the active surface about the x -axis and the y -axis, $p_{x,j}$ and $p_{y,j}$, can be computed by best-fitting the effective surface deviations or the normal displacements through all the surface nodes. The predicted changes in the elevation and azimuth encoder readings $x_{o,j}$ and $y_{o,j}$ are the differences in the calculated rotations between the rotating part and the fixed part of the encoders. The direction of peak gain of the active surface with respect to the encoders are $(p_{x,j}, x_{o,j})$ and $(p_{y,j}, y_{o,j})$.

The predicted displacements and rotations of the subreflector with respect to the best-fitted active surface are computed and their contributions to the direction of peak gain are added. The combined direction of peak gain can be expressed using the following equations (Ref. 5):

$$p_{x,j} = (p_{y,j}, y_{o,j}) - \frac{K_o(\)}{f} - \frac{K_o(\)}{f} u_{s,j} - [K_o(\) + K_o(\)]_{s_{y,j}}$$

$$p_{y,j} = (p_{x,j}, x_{o,j}) - \frac{K_o(\)}{f} - \frac{K_o(\)}{f} v_{s,j} + [K_o(\) + K_o(\)]_{s_{x,j}}$$

where $p_{x,j}, p_{y,j}$ = direction cosine for peak gain in x -axis and y -axis resulting from unit temperature change in member j
 $u_{s,j}, v_{s,j}$ = translation of subreflector vertex along x -axis and y -axis with respect to the best-fitted active surface resulting from unit temperature change in member j
 $s_{x,j}, s_{y,j}$ = rotation of subreflector about x -axis and y -axis with respect to the best-fitted active surface resulting from unit temperature change in member j

For a given set of temperature measurements, the thermal correction model will first extrapolate the temperature for all the members in the telescope structure, and then use the results of the unit temperature load cases to compute the direction of peak gain. The results of the unit temperature load cases combined with the errors in temperature measurement and prediction can be used to evaluate the residual beam pointing error due to thermal effects of the telescope structure after application of the thermal correction model.

THERMAL STUDY

The goal of the thermal design of the telescope is to reduce the temperature differences between different parts of the structure to acceptable levels at all times. This is accomplished by insulating every structural element to the same time constant, enclosing the backstructure, and circulating air inside the backstructure space.

A study was performed to examine the accuracy to which the temperature changes can be obtained by measurement and analysis for a telescope structure in a radome. The thermal study showed that the maximum temperature sensor error is about 0.1°F, and the maximum error in the prediction of the temperature change of any member in the enclosed backstructure is about 0.7°F during the daily

cyclic temperature changes and is about 0.18°F within the two-hour interval between calibrations (Ref. 7).

Based on the above, for the calculation of the residual surface RMS error, an RMS temperature sensor error of 0.05°F and an RMS temperature prediction error of 0.47°F were used for the daily cyclic temperature changes. Therefore, the equivalent RMS temperature error on each individual member was calculated to be 0.47°F (RSS of 0.05°F and 0.47°F).

For the calculation of the residual beam pointing errors, an RMS temperature sensor error of 0.05°F and an RMS temperature prediction error of 0.12°F were used for the two-hour interval between calibrations. Combining both terms, the equivalent RMS temperature error on each individual member was calculated to be 0.13°F (RSS of 0.05°F and 0.12°F).

RESIDUAL SURFACE RMS ERROR OF THERMAL CORRECTION MODEL

As discussed previously, the residual surface RMS error due to thermal effects of the elevation structure after application of the thermal correction model will be due to (a) the error in the temperature measurements, (b) the error in the member temperature predictions, and (c) the error in the temperature effect predictions.

Combining the first two errors to a single equivalent RMS temperature error on each individual member, the residual surface RMS error is the sum of the contributions of all the individual members as follows:

$$RMS^2 = \sum_j \epsilon_j^2$$

where RMS = residual surface RMS error
 ϵ_j = equivalent RMS temperature error for member j

Table 1 shows the residual surface RMS error for $\epsilon_j = 1^\circ\text{F}$ for each of the four thermal loading states. The contributions of different member groups are listed in the table. Among the four thermal loading states, residual surface RMS error is the largest for thermal loading state 4 (bilinear thermal gradient along the z-axis). For $\epsilon_j = 0.47^\circ\text{F}$, the expected residual surface RMS error is about 13.4 μm RMS for thermal loading state 4.

Table 1 - Residual Surface RMS Error RMS / ϵ_j

Member Group	Thermal Loading States			
	RMS / ϵ_j ($\mu\text{m}/^\circ\text{F}$)			
	1	2	3	4
<u>Elevation Structure</u>				
Forward of Hex Ring Beam				
Front Face Members	2.54	4.52	10.08	12.37
Back Face Members	4.02	5.43	8.87	11.44
Posts	1.11	0.86	1.58	2.15
Diagonals	5.28	5.51	7.91	8.43
Transition Structure Forward of Hex Ring Beam	1.74	4.17	6.72	8.80
Subtotal	7.40	9.92	17.04	20.90

Member Group	Thermal Loading States			
	RMS / j (μm/°F)			
	1	2	3	4
Transition Structure (Hex Beam, Drive Arc & Cone)	1.68	7.95	15.17	19.27
Total	7.59	12.71	22.81	28.43

The third error, the error in the temperature effect predictions, is due to errors in modeling and is estimated to be about 5% of the expected surface RMS error predicted by the thermal correction model. The expected surface RMS error to be corrected by the thermal correction model is judged to be about 37 μm for a thermal loading state with a bilinear temperature gradient of 0.011°F/ft below elevation axis and 0.022 °F/ft above elevation axis, resulting in a temperature difference of 3°F over 55 m height of the telescope. Consequently, the modeling error is about 1.9 μm.

Therefore, the residual surface RMS error due to thermal effects of the elevation structure after application of the thermal correction model is expected to be 13.5 μm (RMS) based on RSS of 13.4 μm and 1.9 μm.

RESIDUAL BEAM POINTING ERROR OF THERMAL CORRECTION MODEL

As discussed previously, the residual beam pointing error due to thermal effects of the elevation structure and the alidade after application of the thermal correction model will be due to (a) the error in the temperature measurements, (b) the error in the member temperature predictions within the two hour period, and (c) the error in the temperature effect predictions.

Combining the first two errors to a single equivalent RMS temperature error on each individual member, the beam pointing error is the sum of the contributions of all the individual members as follows:

$$p_{px}^2 = \sum_j p_{x,j}^2$$

$$p_{py}^2 = \sum_j p_{y,j}^2$$

where p_{px} , p_{py} = RMS error in direction cosine for peak gain in x-axis and y-axis
 $p_{x,j}$ = equivalent RMS temperature error for member j

Table 2 - Residual Beam Pointing Errors p_{px} / j and p_{py} / j

Member Group	p_{px} / j (arc sec/°F)	p_{py} / j (arc sec/°F)
<u>Elevation Structure</u>		
Forward of Hex Ring Beam		
Front Face Members	0.52	0.55
Back Face Members	0.70	0.70
Posts	0.14	0.23
Diagonals	0.41	0.53
Transition Structure Forward of Hex Ring Beam	0.38	0.53

Member Group	$\sigma_{px} / \sigma_{py} / \sigma_{\theta_j}$ (arc sec/ $^{\circ}$ F)	$\sigma_{py} / \sigma_{\theta_j}$ (arc sec/ $^{\circ}$ F)
Subtotal	1.05	1.19
Transition Structure (Hex Ring Beam, Drive Arc & Cone)	0.48	1.82
Total	1.15	2.17
<u>Alidade Structure</u>		
Telescope at E = 0 $^{\circ}$	1.95	2.30
Telescope at E = 90 $^{\circ}$	1.66	2.30
<u>Combined Telescope Structure</u>		
Telescope at E = 0 $^{\circ}$	2.26	3.16
Telescope at E = 90 $^{\circ}$	2.02	3.16

Table 2 shows the RMS errors in direction cosines for peak gain for $\theta_j = 1^{\circ}$ F with best-fitting through all actuator support points. The contributions of different member groups are listed in the table. In evaluating the change in the direction of peak gain, values for σ_{θ_j} , $K_o(\theta_j)$, and $K_o(\theta_j)$ corresponding to an illumination function with a 12 dB taper are used (Ref. 5). For $\theta_j = 0.13^{\circ}$ F, the expected RMS error in predictions of direction cosines σ_{px} and σ_{py} are about 0.29 and 0.41 arc sec respectively. Combining the two directions, the RMS residual beam pointing error resulting from temperature measurement and prediction errors is expected to be 0.5 arc sec.

The third error, the error in the temperature effect predictions, is due to errors in modeling and is estimated to be about 5% of the expected pointing correction calculated by the thermal correction model. The expected pointing correction calculated by the thermal correction model is judged to be about 2.1 arc sec in a two-hour period which corresponds to a linear temperature gradient of $\approx 1^{\circ}$ F over 50 m across the telescope. Consequently, the modeling error is about 0.11 arc sec.

Therefore, the RMS residual beam pointing error due to thermal effects of the elevation structure and the alidade after application of the thermal correction model is expected to be 0.51 arc sec based on RSS of 0.5 and 0.11 arc sec. In addition, for the thermal effects of the subreflector support structure, the RMS residual beam pointing error after application of the thermal correction model using a procedure similar to that described above, is estimated to be 0.18 arc sec.

In summary, the residual beam pointing error after application of the thermal correction model is about 0.51 arc sec from thermal effects of the elevation structure and the alidade, and about 0.18 arc sec from thermal effects of the subreflector support structure. The combined RMS error for the thermal correction model is therefore expected to be about 1/2 arc sec.

DISCUSSION

A thermal correction model with a residual surface RMS error of 13.5 μ m (RMS) is compatible with the overall surface error budget of 70 μ m (RMS). Therefore, the use of thermal correction model to account for temperature changes occurring in the elevation structure appears to be a feasible option.

A thermal correction model with a residual pointing error of 1/2 arc sec RMS may be acceptable if the overall pointing budget is relaxed from 0.7 to 1.0 arc sec RMS.

The analysis was performed for a specific antenna configuration, however, the conclusion is applicable to other configurations with similar dimensions and thermal characteristics. The accuracy

of this method depends on the sensitivity of surface accuracy and pointing to a unit change in the temperature of each member, and the accuracy to which the changes of temperature can be determined. Further studies on the final configuration are needed for proof of performance.

There exists a DMAP to compute the effective surface deviation and direction of peak gain of antenna structures, which also allows the user to perform design sensitivity and optimization (SOL 200) of the structure using the above parameters as design responses or constraints. However, in SOL 200, a loading case cannot be used as a design variable. Therefore, the rate of change of surface RMS error and beam pointing error with respect to a unit temperature change of each member has to be computed externally. The process was automated by generating the input for the unit temperature changes through a BASIC program and by submitting MSC/NASTRAN through a BATCH command. A post-processing program was also developed to process the results of 1047 load cases.

CONCLUSION

The performance requirements for the 50-m diameter LMT of 70 μm RMS surface error and 0.7 arc sec RMS pointing error are extremely demanding for such a large aperture. This paper shows that it is feasible to use finite element model and temperature measurements for real time control of active surface and pointing of the telescope to compensate for the thermal deformations of the structure.

In this paper, the residual surface RMS error and pointing error of such a thermal correction model are also estimated.

In this study, MSC/NASTRAN was not only used to compute the effect of the thermal loading on the telescope structure and to obtain the effective surface deviation and direction of peak gain; but was also used to compute the rate of change of the surface RMS error and pointing error for unit temperature change of each member and thereby to obtain the residual surface RMS error and pointing error of the thermal correction model.

ACKNOWLEDGMENTS

The work was performed for the University of Massachusetts partly under direct contract and partly under subcontract to TIW Systems Inc. The authors wish to thank Dr. Joseph Antebi of Simpson Gumpertz & Heger Inc. for his guidance and support.

REFERENCES

1. Nelson, J.E., Mast, T.S., and Faber, S.M., "The Design of the Keck Observatory and Telescope." Keck Observatory Report No. 90, California Institute of Technology, Pasadena, California, January 1985.
2. Zarghamee, M.S., and Antebi, J., "Optimization Sensing and Control in Design of Antennas," *Proceedings of the Twelfth Conference on Analysis and Computation held in conjunction with Structures Congress XIV*, American Society of Civil Engineers, Chicago, Illinois, 15-18 April 1996, pp. 147-153.
3. Antebi, J., Kan, F.W., and Rao, R.S., "Active Segmented Primary and Pointing of the Large Millimeter Telescope (LMT)," *Advanced Technology MMW, Radio, and Terahertz Telescopes*, 26-28 March 1998, *SPIE Proceedings*, Vol. 3357.

4. Nelson J., and Mast T.S. ☞Figure Control of the LMT/GMT Primary Reflector,☞ Report Submitted by TIW Systems Inc. to LMT Project Office, December 1996.
5. Zarghamee, M.S., and Antebi, J., ☞Surface Accuracy of Cassegrain Antennas,☞ *IEEE Transactions on Antennas and Propagation*, Vol. AP-33, No. 8, August 1985, pp. 828-837.
6. Zarghamee, M.S., ☞Minimum Weight Design of Enclosed Antennas by Nonlinear Programming,☞ A Large Radio-Radar Telescope Engineering Studies, Northeast Radio Observatory Corporation, Vol. 1, 30 June 1968, pp. I-126 to I-145.
7. Griffith, P., ☞Thermal Design of the Large Millimeter Telescope (LMT) and Expected Accuracy of Temperatures from Measurements,☞ Report Submitted by Simpson Gumpertz and Heger Inc. to LMT Project Office, December 1997.

